

Phase field simulations of grain growth in two-dimensional systems containing finely dispersed second-phase particles

N. Moelans*, B. Blanpain, P. Wollants

Department of Metallurgy and Materials Engineering, Katholieke Universiteit Leuven, Kasteelpark Arenberg 44, B-3001 Leuven, Belgium

Received 20 April 2005; received in revised form 26 October 2005; accepted 28 October 2005

Available online 15 December 2005

Abstract

The pinning effect of small incoherent particles on grain growth in two-dimensional polycrystalline systems has been simulated using a phase field model. Simulations were performed for different sizes and area fractions of the second-phase particles and for two types of initial microstructure and different initial grain sizes. The grain size distribution and the number of particles located at grain boundaries were determined as a function of time. When particles are present during the nucleation of the grains, most particles are located at grain boundaries and the final mean grain radius \bar{R}_{lim} is predicted by $\bar{R}_{\text{lim}} = 1.28r/f_a^{0.50}$, with r the radius and f_a the area fraction of the particles. When particles nucleate homogeneously in a polycrystalline system with initial grain radius \bar{R}_0 , many particles lie within the grains and the final grain size depends on \bar{R}_0 . It was also observed that the peak of the normalized grain size distribution shifts towards smaller grain sizes due to the pinning effect. The simulation results are compared with theoretical relations, previous simulation results and experimental data for thin films from the literature.

© 2005 Acta Materialia Inc. Published by Elsevier Ltd. All rights reserved.

Keywords: Grain growth; Zener pinning; Phase field models; Simulation; Thin films

1. Introduction

Second-phase particles have the capacity to ‘pin’ grain boundaries and therefore affect the grain growth behavior of polycrystalline materials profoundly. They reduce the mobility of the grain boundaries and eventually, when a critical grain size is reached, arrest grain growth. The existence of a final grain size is of practical importance in alloy development, since many macroscopic properties are related to the grain size. For example, in the manufacturing of high-quality steels, insoluble inclusions or precipitates are often introduced into the material for grain refinement [1,2]. Also in the aluminum films used in micro-electronic devices the pinning effect of small precipitates is applied to tailor the final microstructure [3,4]. To optimize the per-

formance and reliability of these materials, a good understanding of the effect of second-phase particles on the microstructure evolution is required.

The pinning pressure P_Z (pinning force exerted on a unit area of grain boundary) exerted by a distribution of incoherent spherical particles on the grain boundaries was first calculated by Zener [5,6], although in an approximate way:

$$P_Z = \frac{3f_v\sigma_{\text{gb}}}{4r}, \quad (1)$$

r and f_v are, respectively, the radius and the volume fraction of the particles and σ_{gb} is the grain boundary energy. It was assumed that grain boundaries are straight and that particles are randomly distributed. Therefore, only particles within a distance r from the grain boundary contribute to the pinning effect and all contributing particles exert the same pinning force $F_Z = \pi r\sigma_{\text{gb}}$.¹ A stress balance between

* Corresponding author.

E-mail address: nele.moelans@mtm.kuleuven.ac.be (N. Moelans).

URL: nele.studentenweb.org (N. Moelans).

¹ In fact, with these assumptions the interactions between grain boundaries and particles are completely omitted.

the driving force for grain growth and the pinning pressure P_Z results in the Zener relation

$$\frac{\bar{R}_{\text{lim}}}{r} = \beta \frac{1}{f_V^b}, \quad (2)$$

with $\beta = 4/3$ and $b = 1$, which gives the critical maximum grain size as a function of the volume fraction and the mean radius of the second-phase particles. To obtain a more accurate description, the characteristic ‘dimple’ shape of a grain boundary near a grain boundary-particle intersection was considered [7], mainly resulting in a lower value for β . A relation of the same form as (2) was obtained with $\beta = 2/9$ and $b = 0.93$. It was observed that for high volume fractions most particles are located at grain boundaries, whereas for low volume fractions the distribution of the particles (with respect to the grain boundaries) is more random. In [8], relation (2) with $\beta = 1.8$ and $b = 1/3$ was therefore proposed for high volume fractions in combination with $\beta = 2/9$ and $b = 0.93$ for low volume fractions. For two-dimensional systems, $\beta = \sqrt{3}$ and $b = 1/2$ was obtained assuming that stagnation occurs when there is a particle at each grain boundary [9]. Many more attempts were made to improve the Zener relation [6,10,11]. However, calculation of the pinning pressure exerted by a distribution of particles is extremely complex [6], since it requires the knowledge of the number of particles located at grain boundaries and the geometry of each grain boundary-particle intersection. Simplifying assumptions were always necessary and most theories resulted in a relation similar to the Zener relation.

From mean field theory, the following equation was obtained for the growth rate of a single grain in a material containing second-phase particles [12],

$$\frac{dR}{dt} = cM\sigma_{\text{gb}} \left(\frac{1}{R_{\text{crit}}} - \frac{1}{R} \pm \frac{P_Z}{c\sigma_{\text{gb}}} \right). \quad (3)$$

M is grain boundary mobility and c is a dimensionless constant. The negative sign applies for large grains with $1/R < 1/R_{\text{crit}} - P_Z/c\sigma_{\text{gb}}$ and the positive sign for small grains with $1/R > 1/R_{\text{crit}} + P_Z/c\sigma_{\text{gb}}$. Between these two limits $dR/dt = 0$. R_{crit} is related to the mean grain radius and P_Z is the pinning pressure of the particles. Relation (3) in combination with a continuity equation (expressing that grains have to be space filling) gives

$$\frac{d\bar{R}^2}{dt} = \frac{c}{2} M\sigma_{\text{gb}} \left(1 - \frac{P_Z \bar{R}}{c\sigma_{\text{gb}}} \right)^2, \quad (4)$$

for the temporal evolution of the mean grain radius. The relation describes a growth rate that is initially parabolic, subsequently decreases and eventually stagnates. It was also derived from Eq. (3) [13,14] that, due to the pinning effect, the normalized grain size distribution becomes sharper and its peak shifts towards smaller grain sizes during grain growth.

Experimental data on Zener pinning are too limited and scattered to conclude on the validity of the different

assumptions [10]. Therefore simulations, mainly Monte Carlo (based on a Potts model) [9,15–20] and front-tracking (based on a vertex model) [21,22] simulations, were performed to study the pinning effect of particles on grain growth in more detail. The major advantage of simulations is that no assumptions must be made about the number of particles interacting with grain boundaries and the grain boundary geometry at a grain boundary-particle intersection. However, if the simulation grid is too coarse to resolve the grain boundary shape appropriately or if the system size is too small, simulation results may be incorrect [17,23,24]. Adequate computer resources and long computation times are therefore required. The simulations show that the fraction of particles located at grain boundaries is considerably larger than assumed in the Zener relation and increases with the volume fraction of the particles. Furthermore, many particles pin the vertices where grain boundaries intersect, which is more effective than pinning a single grain boundary. It was also noticed that the pinning effect in two-dimensional (2D) systems is stronger than in three-dimensional (3D) bulk materials, mainly because in 2D systems grain boundaries have the tendency to become straight in between the particles [8,25]. Thus, it is more difficult for the grain boundaries to escape from the particles, since all driving pressure for grain boundary movement is removed once a grain boundary is straight. Most 2D simulations [9,16–19,21,22] confirm that the volume fraction exponent b is approximately 0.5. For 3D systems, there is less agreement. In [15,17] simulations for $0.005 < f_V < 0.16$ gave values for b close to $1/3$, whereas in [20], b equal to one was obtained for $0.025 < f_V < 0.15$.

Today the phase field method is developing as a versatile tool for simulating microstructure evolution phenomena, such as solidification, precipitation and grain growth. Grain growth in single-phase materials has been simulated several times with the phase field method [26–29]. An extension of the model of [26] towards grain growth in two-phase materials was given in [30,31] and 2D phase field simulations for Zener pinning by growing second-phase particles were discussed in [32]. In [32] simulations were performed for volume fractions of the second-phase between 0.1 and 0.4 and \bar{R}/\bar{r} -ratios (the ratio between the mean grain radius and the mean particle radius) smaller than 4.4. However, in many materials $f_V < 0.1$ and particles can be more than 100 times smaller than the grains. Then the model of [32] is too computationally intensive.

In a previous article, we presented a different phase field model for grain growth in the presence of second-phase particles which have a size and shape that is constant in time [33]. The interaction between a single particle and a grain boundary was also shown. In this article 2D phase field simulations for Zener pinning in polycrystalline systems are presented. Simulations were performed for different area fractions and sizes of the particles and for two types of initial microstructure and different initial grain sizes. The results are compared with relation (2), previous simulation results and experimental data for Al-alloy films. Furthermore,

computational requirements are discussed and an estimation of the requirements for 3D simulations is made.

2. Phase field model

According to the phase field model for grain growth in single-phase materials of [26], a large number of phase field variables

$$\eta_1(\mathbf{r}, t), \eta_2(\mathbf{r}, t), \dots, \eta_p(\mathbf{r}, t),$$

is used to distinguish the different orientations of the matrix grains. They are continuous functions of the spatial coordinates and the time. Within a grain labelled by η_i , η_i equals 1 or -1 , while all other phase field variables equal 0. At a grain boundary all η_i vary continuously between their equilibrium values in the neighbouring grains. A spatially dependent function Φ that equals 1 inside a particle and 0 in the matrix grains is used to describe the distribution of the particles. Φ is considered to be constant in time.

The free energy of the system is described by the expression

$$F = \int_V \left[m \left(\sum_{i=1}^p -\frac{1}{2} \eta_i^2 + \frac{1}{4} \eta_i^4 + \sum_{i=1}^p \sum_{j \neq i}^p \eta_i^2 \eta_j^2 \right) + \epsilon \Phi \sum_{i=1}^p \eta_i^2 + \sum_{i=1}^p \frac{\kappa_i}{2} (\nabla \eta_i)^2 \right] d^3 \mathbf{r}. \quad (5)$$

The first four terms give the contribution due to bulk free energy. m and ϵ are positive constants, with $\epsilon > m/2$ so that for $\Phi = 0$ the local free energy has $2p$ minima with equal depth, located at

$$(\eta_1, \eta_2, \dots, \eta_p) = (1, 0, \dots, 0), (0, 1, \dots, 0), \dots, (0, 0, \dots, 1), \\ (-1, 0, \dots, 0), (0, -1, \dots, 0), \dots, \\ (0, 0, \dots, -1),$$

reflecting the $2p$ orientations a matrix-grain can have, and for $\Phi = 1$ the local free energy has one minimum at all η_i equal to 0. The last term, with all κ_i positive constants, is a contribution due to local gradients of the phase field variables. It only differs from zero at the grain boundaries and particle–matrix interfaces.

The phase field variables η_i are non-conserved. Their spatial and temporal evolution is obtained by solving a time-dependent Ginzburg–Landau equation for each variable η_i , $i = 1, 2, \dots, p$,

$$\frac{\partial \eta_i(\mathbf{r}, t)}{\partial t} = -L_i \frac{\partial F}{\partial \eta_i(\mathbf{r}, t)} \\ = -L_i \left[m \left(-\eta_i + \eta_i^3 + 2\eta_i \sum_{j \neq i}^p \eta_j^2 \right) + 2\epsilon \eta_i \Phi^2 - \kappa_i \nabla^2 \eta_i \right]. \quad (6)$$

L_i are kinetic coefficients that are related to the grain boundary mobility. We refer to [33] for a complete description of the model.

For isotropic grain boundary energy and mobility $\kappa_i = \kappa$ and $L_i = L, \forall i$. Then grain boundary energy is proportional to $\sqrt{\kappa m}$ and grain boundary thickness to $\sqrt{\kappa/m}$. For a given value of κ and m , interfacial energy of the particles depends on ϵ , however ϵ can only vary within a small range. For normal grain growth, growth rate is proportional to $L\kappa(1/R)$, with R the local mean curvature of the grain [28]. In [33] grain boundary and interfacial energies were calculated for different values of the parameters κ , m and ϵ .

To consider the growth and dissolution of particles, for example to simulate Ostwald ripening, at least one conservative variable related to the local composition must be added to the set of phase field variables. The spatial and temporal evolution of a conservative phase field variable is described by a Cahn–Hilliard equation, which contains fourth order derivatives of the phase field variable to the spatial coordinates. As a consequence, the numerical solution is considerably more complicated. In the model of [32], beside the set of phase field variables for the matrix grains and a concentration variable, a second set non-conservative phase field variables is used to distinguish the different orientations of the particles. However, when particles are finely dispersed and interfacial properties are isotropic, the orientation of the particles is not important. Moreover, in some cases the coarsening of the particles is negligible, for example at temperatures where the solubility of the second phase is very low [34].

3. Model parameters and simulation procedure

The number of parameters was restricted to a minimum and their choice was mainly based on computational considerations and previous phase field simulations for normal grain growth [28]. Thirty-six phase field variables were used to represent the polycrystalline matrix. κ was chosen equal to 0.5 and L , m and ϵ equal to 1. Periodic boundary conditions were assumed and a semi-implicit Fourier-spectral method [35] was employed for the numerical solution of the phase field Eq. (6). The grid spacing Δx was taken equal to one. For the parameter values given above, the semi-implicit Fourier-spectral method allows a step size Δt equal to 1. In the further discussion, length and area are expressed in number of grid points (g.p.) and time in number of time steps (t.s.). In [28] it was shown that κ/m should be at least 4 (for $\Delta x = 1$) to resolve the evolution of the phase field variables at grain boundaries appropriately and to obtain the correct rate of grain growth. However, grain boundary thickness is then more than 10 g.p. As a compromise between accuracy and efficiency, κ/m equal to 0.5 was applied in the simulations.

According to the Zener relation (2), the final grain size is proportional to the particle size for a given area fraction. Consequently, it is better to not take the particle size too large, so that system size is restricted. On the other hand, particles must have a minimum size, that depends on the grain boundary thickness, to obtain realistic grain boundary–particle interactions [33]. Therefore, particles

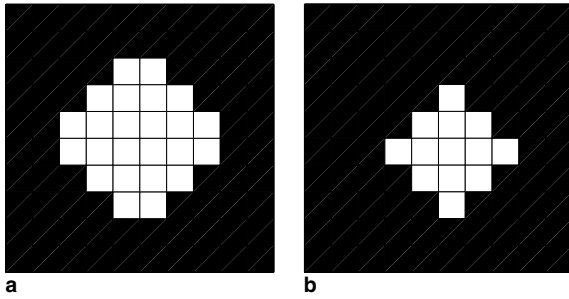


Fig. 1. Discretized shape of the particles used in the simulations: (a) $r = 3$ and (b) $r = 2.5$. White represents $\Phi = 1$ and black $\Phi = 0$.

with radius 2.5 and 3 g.p. were used. Φ was only determined in the discrete grid points: it equals one at grid points within particles and zero at the other grid points. For both particles the representation by Φ is shown in Fig. 1.

To obtain a fine grained microstructure, small random values between -0.001 and 0.001 were assigned to the phase field variables at all grid points and then phase field variables were allowed to evolve according to Eq. (6). After about 50 time steps the grains impinge. In a first set of simulations (further referred as $\bar{R}_0 = 0$), particles were present during the nucleation of the grains. Then most of the particles end up at grain boundaries. The simulations correspond, for example, to grain growth after solidification of a melt containing solid particles, or to grain growth in thin films with second-phase particles prepared by electrolytic co-deposition. In a second set of simulations (further referred as $\bar{R}_0 > 0$), the role of the initial grain size was studied. Grain nucleation and initial grain growth occurred first without particles. When the mean grain size equaled a specified initial grain size \bar{R}_0 , particles were randomly distributed throughout the system. As a consequence, many particles lie within grains. These simulations correspond to the case where grain growth follows homogeneous precipitation or recrystallization.² The time step when particles are added is always considered as the beginning ($t = 0$) of the experiment.

Area fractions between 0.004 and 0.16 and initial grain sizes up to 40.8 were considered. A few simulations for single-phase system were also implemented. System sizes were 256×256 , 512×512 and 1024×1024 g.p. An IBM Pseries 630 with power4 processors of 1 GHz and 4 GB RAM was used to run the simulations. The MATLAB[®] programming language allows an efficient implementation of the Fourier-spectral method [36].

4. Simulation results

Fig. 2 shows the grain growth evolution for both types of initial microstructure. The function Ψ , defined as

$$\Psi(\vec{r}) = \sum_{i=1}^p \eta_i^2(\vec{r}), \quad (7)$$

is displayed using grey-levels with white representing $\Psi = 1$ and black $\Psi = 0$. Particles appear as black spots, grains are bright and grain boundaries grey. The radius of a grain is calculated as $R = \sqrt{A/\pi}$, with A the number of grid points within the grain. The initial microstructure for a system where particles were present before nucleation of the grains ($\bar{R}_0 = 0$) is displayed in Fig. 2(a). Initially all particles are located at grain boundaries. The Fig. 2(b)–(d) show that during grain growth the grain boundaries can escape from some of the particles. However, grain boundaries easily become straight and therefore lack the driving pressure to pass the particles. As a consequence, most of the particles are still located at grain boundaries in the final microstructure, where all grain boundaries are straight. When particles nucleate after grains have formed ($\bar{R}_0 > 0$), initially many particles are located within the grains (Fig. 2(e)), but the number of particles on grain boundaries increases during grain growth (Fig. 2(f)–(h)). The grain boundaries are pinned by the particles they meet, whereas unpinning is more difficult because the grain boundaries have the tendency to become straight in between the particles. Nevertheless, at the end, when grain growth has arrested, there are still more particles located within grains than is the case for $\bar{R}_0 = 0$, in Fig. 2(d). Although the size and area fraction of the particles are the same, the final grain size is larger and the time before grain growth arrests, is longer for $\bar{R}_0 > 0$. Thus the simulations show that the pinning effect of the particles depends on initial grain boundary configuration and initial grain size.

In Fig. 3 the mean grain area is plotted as a function of time for several simulation experiments. For pure single-phase materials the temporal evolution follows the power growth law

$$\bar{R} = k * t^n, \quad (8)$$

with $n = 0.5$ [10]. The mean grain area increases linearly in time, accordingly. When particles are present, the growth rate reduces gradually and finally becomes zero. In general, grain growth stops earlier and the final grain size is smaller for larger area fractions of the second phase, which is in qualitative agreement with mean field predictions [10,12]. Further, the final grain size increases with initial grain size and the time before grain growth arrests is also longer for a larger initial grain size. The form of Eq. (4) does not allow an easy fit of the simulation data. However, for $R_0 = 0$ grain growth behavior can be quantified as follows (Fig. 3(c)). In the beginning grain growth is according to the power growth law with n between 0.3 and 0.4. The value of n is highly related to the number of particles per unit of area. For a system of 512×512 g.p. containing 80 particles n equaled 0.4 for both particle sizes, for 160 particles n equaled 0.37. Then there is a clear transition to growth stagnation where the grain size is constant. For $\bar{R}_0 > 0$ such a period of steady-state growth according to a power

² Because the driving pressure for recrystallization is much larger than for grain growth, grain boundaries can more easily pass particles [10] resulting in a large number of particles within the grains.

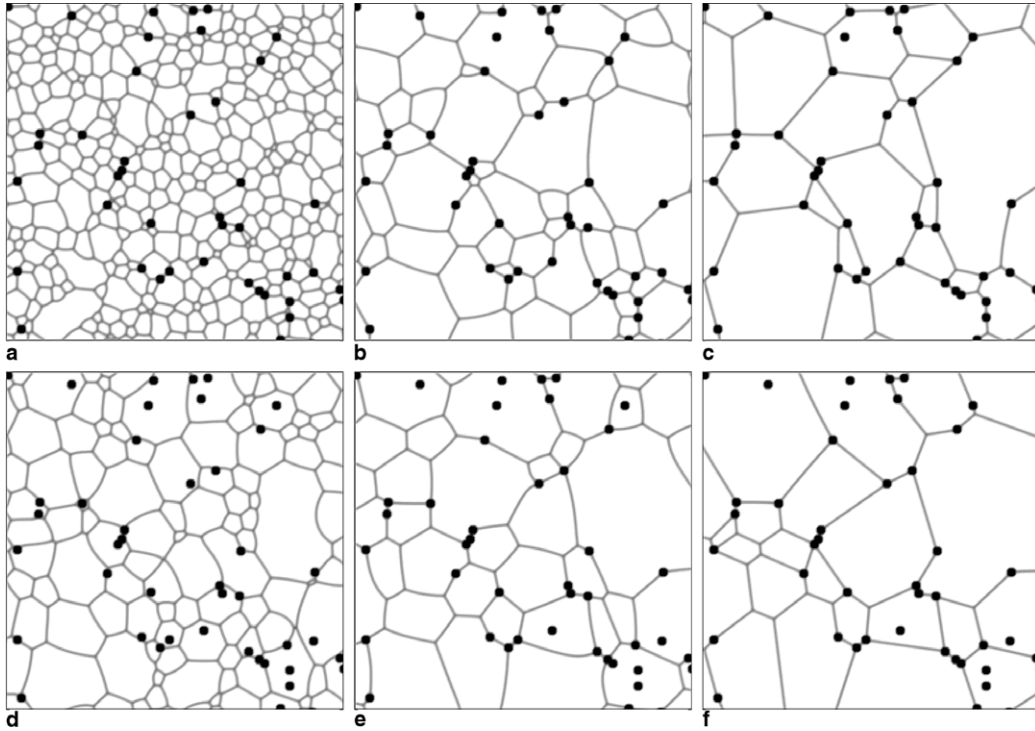


Fig. 2. Evolution of a polycrystalline system containing second-phase particles for $r = 3$ and $f_a = 0.015$. (a–c) Particles were present during nucleation of the grains ($\bar{R}_0 = 0$). Microstructures at time steps (a) 200, (b) 3000 and (c) 30,000 are shown. No further evolution was observed after approximately 30,000 time steps, where $\bar{R}_{lim} = 29.5$. (d–f) Particles nucleated when the grain radius equaled $\bar{R}_0 = 14.4$. Microstructures at time steps (d) 5, (e) 3000 and (f) 35,000 are shown. No further evolution was observed after approximately 35,000 time steps, where $\bar{R}_{lim} = 32.3$.

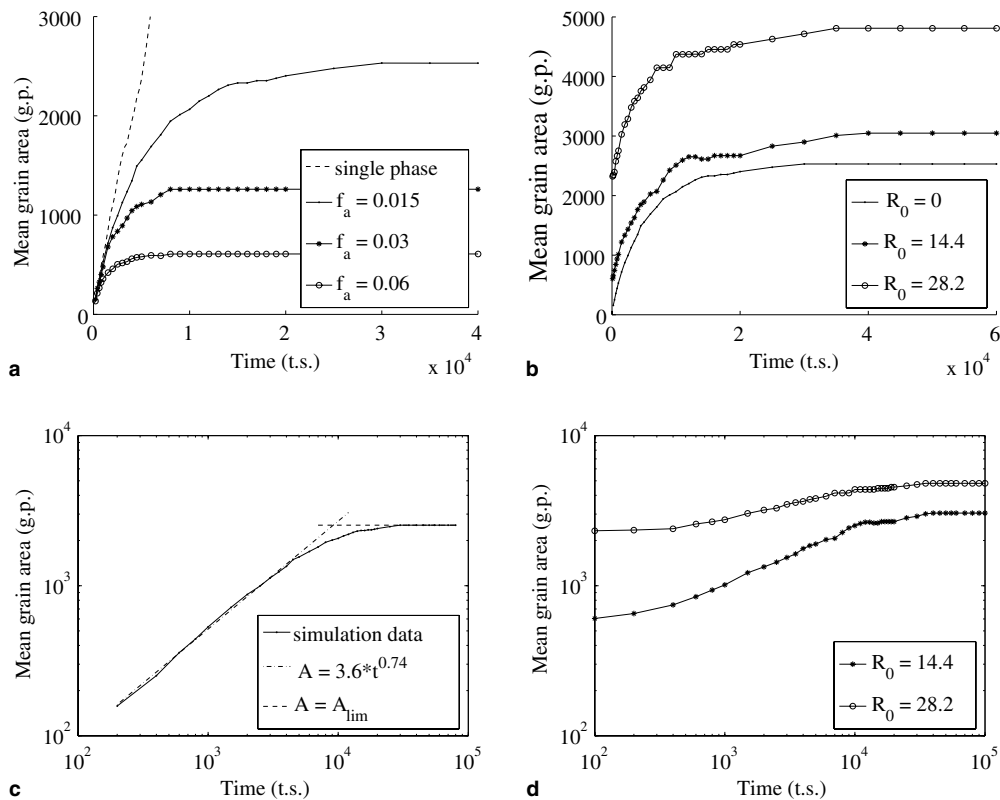


Fig. 3. Temporal evolution of the mean grain area in systems containing second-phase particles. (a) $R_0 = 0$, $r = 3$ and different area fractions of the particles f_a , compared with the evolution of the mean grain area in a single-phase system. (b) $r = 3$, $f_a = 0.015$ and different initial grain sizes \bar{R}_0 . (c) and (d) $r = 3$, $f_a = 0.015$ and different initial grain sizes, (c) $\bar{R}_0 = 0$ and (d) $\bar{R}_0 > 0$, on a logarithmic scale.

growth law is not present or is very short. 2D Monte Carlo simulations for $R_0 = 0$ [9] show a more abrupt transition from growth according to the power growth law with $n = 0.4$, to stagnation. For front-tracking simulations [21,22], n equals 0.5 as long as only a small number of particles interact with the grain boundaries and then gradually decreases. According to the authors' knowledge, there is no systematic experimental information that allows the verification of Eq. (4) and the simulation results.

For all simulations, the ratio of the final mean grain radius and the particle radius, is plotted as a function of second-phase area fraction in Fig. 4. There is a considerable scatter on the results for $f_a < 0.01$, since the number of particles considered in one simulation and the number of grains in the final microstructure are rather low (often less than 50). Due to restrictions in computer memory it was not possible to increase the system size above 1024×1024 g.p. Therefore, in order to have a reliable value for the final grain radius, the average over all simulation experiments for a particular particle size and area fraction must be taken. The systems contain enough grains to assume that boundary effects are negligible.

The simulation results for $\bar{R}_0 = 0$ fit relation (2) for $\beta = 1.28(\pm 0.15)$ and $b = 0.50(\pm 0.02)$ very well. The coefficients were obtained from a linear least squares fit of the $\log(f_a) - \log(\bar{R}_{\text{lim}}/r)$ data points. The number between brackets indicates the 95% confidence limits. The adjusted R^2 value was 0.98. The relation is in good agreement with the theoretical relation for 2D from [9] ($\beta = \sqrt{3}$ and $b = 0.5$) and with relations previously obtained from simulations. Monte Carlo simulations gave, for example, $\beta = \sqrt{2.9}$ and $b = 0.5$ [9] or $\beta = 1.2$ and $b = 0.55$ [16], and front-tracking simulations gave $b = 0.5$ [21] or $b = 0.46$ [22] (β was not determined). Presuming $b = 0.5$, the phase field simulations in [32] gave $\beta = 1.3$ for

$f_a < 0.3$. For $f_a > 0.3$, results were affected by clustering of the particles. All relations are plotted in Fig. 5. Our relation is very close to the relation from [32]. Due to the diffuse interfaces the pinning force of a particle is slightly too high in phase field simulations [33], which may result in a lower value for β . This probably explains why both curves obtained from phase field simulations are below those obtained from Monte Carlo simulations. For Monte Carlo simulations it was observed [17] that β may depend on the numerical grid, as the grid unit affects the discretized shape of small particles. Thanks to the diffuse character of the interfaces, this discretization artefact seems to be insignificant for phase field simulations. Although both particles used in the present simulations are slightly different in shape after discretization (see Fig. 1) and are also different from the growing particles in [32], almost the same relation is obtained.

The simulation results for $\bar{R}_0 > 0$ show that for high area fractions of the particles the final mean grain radius is considerably affected by the initial microstructural configuration. For a given area fraction and size of the particles, the final grain size increases with initial grain size. For low area fractions, the influence of the initial microstructure is negligible. A fit of the data shows that β increases and b decreases in relation (2) for increasing initial grain size: $\beta = 1.9(\pm 0.5)$ and $b = 0.43(\pm 0.09)$ was obtained for $\bar{R}_0 \approx 14.4$ (adjusted $R^2 = 0.95$) and $\beta = 4.4(\pm 1.0)$ and $b = 0.28(\pm 0.07)$ for $\bar{R}_0 \approx 28.2$ (adjusted $R^2 = 0.92$). Thus, the coefficients in relation (2) depend on the initial configuration. However, the adjusted R^2 values indicate that a relation of the form (2) is less appropriate for high initial grain sizes. In the limit of large initial grain size and high area fraction, the final grain size becomes independent of the area fraction. Grain boundaries then merely adapt their shape in order to intersect

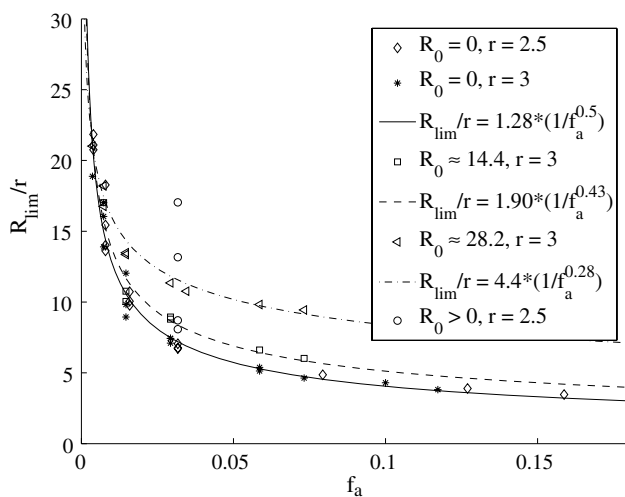


Fig. 4. Final grain radius \bar{R}_{lim} divided by particle radius r as a function of area fraction of the particles f_a for different initial grain sizes: $\bar{R}_0 = 0, 14.4$ and 28.2 . A series of data points for a constant particle size $r = 2.5$ and area fraction $f_a = 0.032$ and increasing initial grain size \bar{R}_0 , is also plotted: $\bar{R}_0 = 10.9, 14.4, 28.0$ and 40.8 .

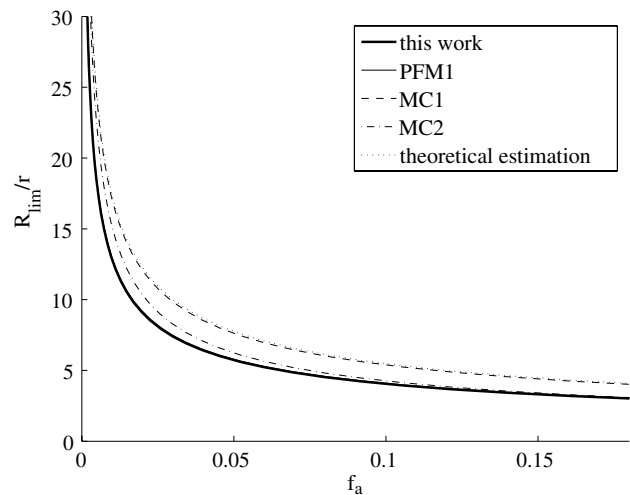


Fig. 5. Zener type relations obtained from different 2D simulation experiments and from a theoretical estimation: present phase field simulations, phase field simulations from [32] (PFM1), Monte Carlo simulations from [9] (MC1) and [16] (MC2), theoretical relation assuming that at grain growth stagnation there is a particle at each grain boundary [9].

as many particles as possible, but the mean grain size hardly increases, as is illustrated in Fig. 6. Similar observations were reported for Monte Carlo [18] and front-tracking [21] simulations for systems with many particles inside the grains.

Fig. 7 gives the temporal evolution of the normalized grain size distribution for a system containing second-phase particles. The normalized grain size distribution obtained for a single-phase system is also shown for one particular time step, as it is known that for single-phase systems the normalized grain size distribution is constant in time. The grain size distributions were obtained from systems with 1024×1024 g.p., so that at the end of the simulation there were still 454 grains in the system. The simulation results show that due to the second-phase particles the peak of the normalized grain size distribution shifts towards smaller grain sizes, as predicted by mean field theories [12–14]. However, for high area fractions of the second-phase particles ($f_a > 0.1$), the shift is less significant. This observation is different from the findings from 2D Monte Carlo simulations [9] where the normalized grain size distribution was not significantly affected by the particles. For front-tracking simulations [21,22], on the other hand, a shift towards smaller grain sizes was reported and it was also observed that the effect diminishes for high pinning forces. This behavior of the grain size distribution can be explained as follows. Since the local driving force for a grain boundary to move forward is proportional to its curvature, large grains are often pinned more easily than small grains. As a consequence, the shape of the grain size distribution changes during grain growth. However, for high pinning forces, grain growth is arrested before the grain size distribution is modified significantly. Only few experimental studies of the influence of second-phase particles on the shape of the grain size distribution exist. Some [14,37] indicate a shift towards smaller grain sizes, whereas for others [38] the shape of the grain size distribution is not affected by the particles.

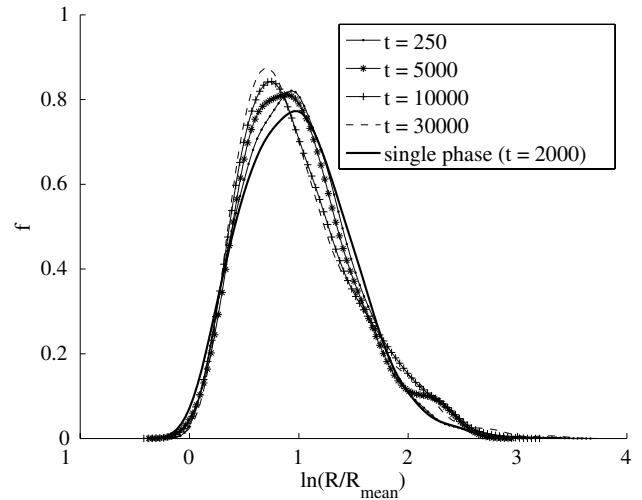


Fig. 7. Normalized grain size distribution at different time steps for a system containing second-phase particles ($f_a = 0.02$, $r = 3$ g.p.) compared with the normalized grain size distribution for a single-phase system.

5. Discussion

5.1. Role of the initial grain size

To understand the role of the initial grain size, the fraction of particles located at grain boundaries ϕ as a function of time is plotted in Fig. 8 for both types of initial microstructure. When particles are present during nucleation of the microstructure ($R_0 = 0$), in the beginning most particles lie on the grain boundaries ($\phi \approx 1$). As grain growth proceeds, ϕ decreases in time because the grain boundaries escape from some of the particles, often leaving the particle behind within a grain. The decrease in ϕ is smaller for high area fractions since unpinning is more difficult when a grain boundary is pinned by many particles. When particles are homogeneously distributed throughout a system with initial grain radius $\bar{R}_0 > 0$, initially there is no correlation between the position of the particles and the grain

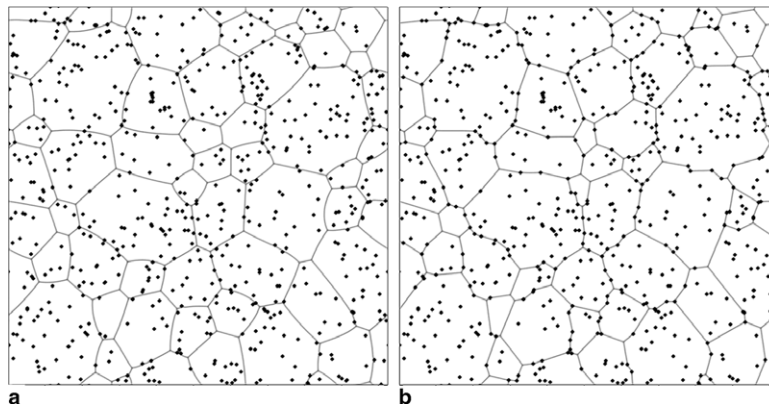


Fig. 6. Evolution of a microstructure after precipitation of a random distribution of second-phase particles ($f_a = 0.032$, $r = 2.5$) at large initial grain size. (a) Initial microstructure ($\bar{R}_0 = 40.8$). (b) Final microstructure ($\bar{R}_{lim} = 42.6$).

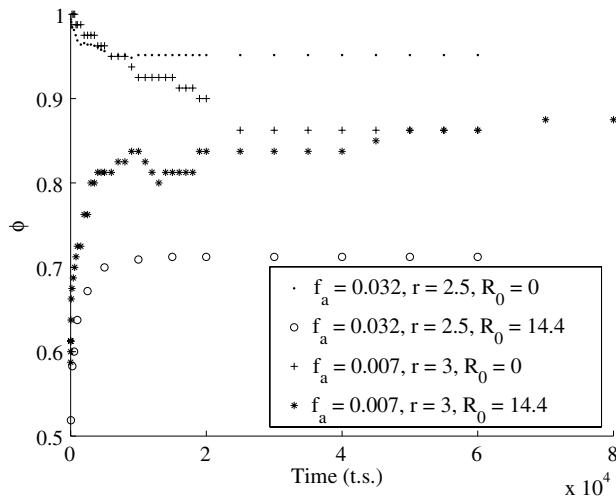


Fig. 8. Fraction of particles located at grain boundaries ϕ as a function of time, for different area fractions f_a of the second-phase particles and different initial grain sizes \bar{R}_0 of the matrix phase.

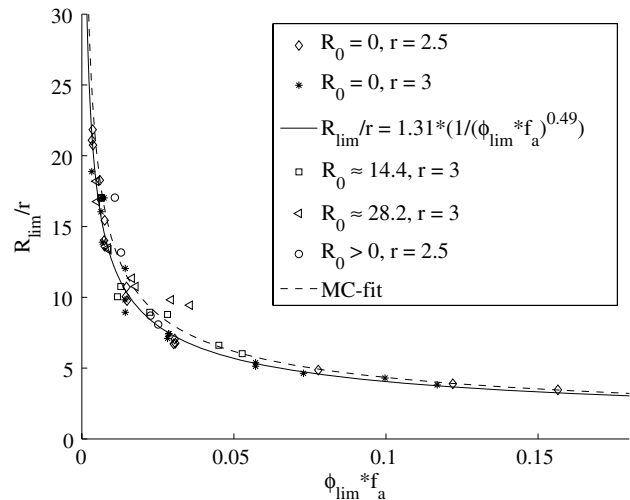


Fig. 9. \bar{R}_{lim}/r as a function of the area fraction of the particles f_a multiplied by the fraction of particles located at grain boundaries in the final microstructure ϕ_{lim} . A fit of the data points for $\bar{R}_0 = 0$ and the relation obtained from Monte Carlo simulations [19] are added.

boundaries. Many particles lie within the grains and $\phi \ll 1$. Since the moving grain boundaries get pinned by the particles they meet, ϕ increases in time. For high area fractions or large initial grain sizes, particles located in the middle of a grain have a low probability to be passed by a grain boundary. The mean grain size exceeds the final mean grain size obtained for $\bar{R}_0 = 0$ before ϕ reaches the final value ϕ_{lim} , observed for $\bar{R}_0 = 0$. For low area fractions or when the initial grain size is small, the probability that a particle within a grain is passed by a grain boundary is higher and at the end ϕ reaches the same value as in the simulations for $\bar{R}_0 = 0$. Therefore, the role of the initial grain radius is negligible for very low area fractions and becomes increasingly important for higher area fractions and larger initial grain sizes.

Except for [18,21,25], the role of the initial grain size has rarely been mentioned in literature. Sometimes [8,39] the fraction of particles located at grain boundaries in the final microstructure ϕ_{lim} is treated as an extra parameter to avoid approximations in calculating the number of particles contributing to the pinning effect. For Zener pinning in 2D, f_a was multiplied by ϕ_{lim} in relation (2) with $\beta = \sqrt{3}$ and $b = 0.5$ [8]

$$\frac{\bar{R}_{\text{lim}}}{r} = \beta \frac{1}{(\phi_{\text{lim}} f_a)^b}, \quad (9)$$

to correct for the fact that not all particles are located at grain boundaries. Results from 2D Monte Carlo simulations [19] gave a very good fit for relation (9) with $\beta = 1.34$ and $b = 0.51$. However, in these simulations particles were present during nucleation of the grains and ϕ_{lim} was always larger than 0.8. A fit of our simulation data for $\bar{R}_0 = 0$ gave $\beta = 1.31(\pm 0.12)$ and $b = 0.49(\pm 0.02)$. The adjusted R^2 value was 0.98, indicating a quite good fit. Fig. 9 shows that the $\phi_{\text{lim}} f_a - \bar{R}_{\text{lim}}/r$ data points for $\bar{R}_0 > 0$ are closer to those for $\bar{R}_0 = 0$ than is the case for

the $f_a - \bar{R}_{\text{lim}}/r$ data points in Fig. 4. For large initial grain sizes, nonetheless, the equation is not able to truly account for the influence of the initial microstructure. In [18,40] a stereological parameter \mathbf{R} , related to the degree of contact between grain boundaries and second-phase particles in the final microstructure was included into the Zener relation. Anyway, these theories are not very useful for prediction of the final mean grain radius, as they require the knowledge of ϕ_{lim} or \mathbf{R} , both properties of the final microstructure.

From a thermodynamic point of view, it is evident that the initial microstructure must be considered as well, since grain growth stagnation is a metastable equilibrium. Real thermodynamic equilibrium, where the total free energy is minimal, consists of one matrix grain with all the particles inside. As there may be multiple metastable equilibria, the final microstructure depends on the initial microstructure and its evolution. Relations of the form (2) are based on a balance of all forces exerted on the grain boundaries, but do not consider the evolution of the microstructure. Therefore, they are not able to predict which of the metastable equilibria will be reached and numerous assumptions about the mutual distribution of particles and grain boundaries in the final microstructure have to be made to calculate the forces. Techniques, such as phase field or Monte Carlo simulations, combine thermodynamics and kinetics and describe the complete evolution of a microstructure. They can predict towards which metastable equilibrium a microstructure will evolve. This capacity is an important advantage, as grain growth can follow various microstructural processes, such as solidification or recrystallisation. Depending on the processing route of a material and the further treatments, various microstructures may be developed before grain growth starts.

In 3D systems a grain boundary can more easily escape from particles [8,33]. The influence of the initial

microstructure is therefore probably less in bulk materials, however still present for high volume fractions of the particles or large initial grain sizes. This may be one of the reasons for the scatter on the experimental data for relation (2) and for the choice of $b = 1/3$ instead of $b = 1$ at high volume fractions [8].

5.2. Comparison with experiments

The simulation results are compared with experimental data for Al-films containing Θ' -CuAl₂ precipitates [4] in Fig. 10. The Θ' -CuAl₂ precipitates were disc shaped and lay primarily in the middle of the film parallel with the plane of the film. Further, the grains were columnar, with their grain boundaries perpendicular to the plane of the film. Hence, grain growth behavior and the interaction with the particles is 2D. The experimental points lie systematically above the relation obtained for $\bar{R}_0 = 0$. A first explanation is that many particles are located within grains and consequently do not contribute to the pinning effect. However, there are many more parameters that could have influenced the final grain size. Phenomena such as surface grooving at grain boundaries and the preferential growth of grains that have an orientation with low surface energy, always occur in thin films [41]. Surface grooving contributes to the pinning of grain boundaries, whereas preferential growth due to surface energy anisotropy leads to abnormal grain growth. Furthermore, the Θ' -CuAl₂ precipitates were semi-coherent, what may have affected the grain boundary geometry at a grain boundary-particle intersection and the pinning strength of the particle distribution, mainly resulting in a higher value of β [6,42].

5.3. Computational considerations

For 2D systems the available computer resources allowed the reproduction of the \bar{R}_{lim}/r -values that were experimentally measured for the Al-films, although compu-

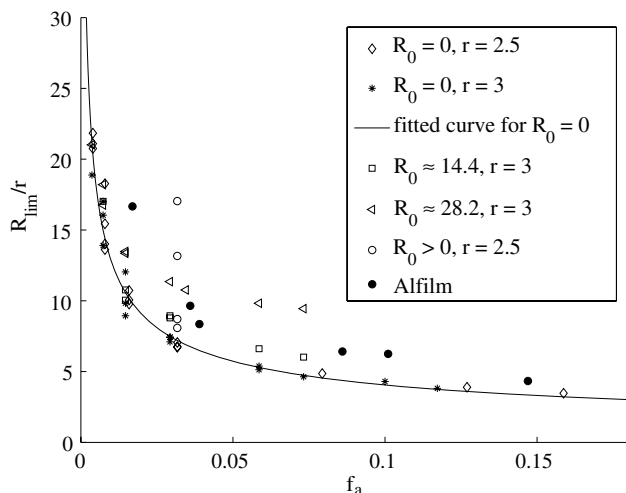


Fig. 10. Phase field results compared with experimental data for Al-films containing Θ' -CuAl₂ precipitates [4].

tation times were long. For high area fractions, $f_a > 0.05$, systems of 256×256 g.p. were used and grain growth arrested after about 20,000 time steps. Then, the simulation time was approximately 10 h. For low area fractions, system size had to be at least 512×512 g.p. and it could take up to 120,000 time steps before grain growth arrested, since at the end grain growth became very slow. Such simulations lasted for approximately 20 days. For the largest systems with 1024×1024 g.p. the memory requirements were close to the maximum available and it took approximately 8 days per 10,000 time steps.

In principle, the same phase field model can be used for 3D simulations. There are unfortunately two major complications that enormously increase the computer requirements. Firstly, the \bar{R}_{lim}/r -ratios observed for 3D systems are typically 10 times larger than for 2D systems. The system size must accordingly be 10 times larger in each dimension. Secondly, in 3D the total number of grid points is proportional to the third power of the system size. As a result, the number of grid points required to obtain a reliable value of the final grain size is roughly 10^5 times larger than for the current 2D simulations. Computer memory requirements and calculation times increase so drastically that simulations must be performed on a cluster of supercomputers, using a parallel code.

6. Conclusion

The pinning effect of randomly distributed second-phase particles was studied by 2D phase field simulations. To cut down on computer requirements, a spatially dependent parameter that is constant in time was used to describe the particle distribution, instead of a large set of phase field variables. This strong reduction of the number of phase field variables allows to perform, on a single computer, 2D simulations for a wide range of area fraction of the particles and for \bar{R}_{lim}/r -ratios up to 20, as observed for Al-films. Grain growth was studied for two types of initial microstructure:

- When particles are present during nucleation of the grains, most particles lie on grain boundaries and the final grain size follows a Zener type relation

$$\frac{\bar{R}_{\text{lim}}}{r} = 1.28 \frac{1}{f_a^{0.50}}. \quad (10)$$

Grain growth can be characterized by growth according to a power growth law with n between 0.3 and 0.4 at the beginning, followed by a gradual, though clear, transition to growth stagnation.

- When particles precipitate homogeneously in a system with initial grain size \bar{R}_0 , many particles lie within the grains. For high area fractions, the final grain size then also depends on \bar{R}_0 . The onset of growth stagnation is less defined and the time before stagnation is longer for a larger initial grain radius.

Furthermore, it was seen that due to the pinning effect the peak of the normalized grain size distribution shifts towards smaller grain sizes. The influence of grain boundary energy and interfacial energy associated with the grain boundary–particle interface was not studied. However, in the simulations of [32] grain boundary energy did not affect the final grain size and in [6] it was pointed out that, for ideal spherical and incoherent particles, the final grain size is independent of grain boundary energy and interfacial energy of the particles.

Simulation techniques, such as phase field and Monte Carlo, describe the complete evolution path of a microstructure and can therefore predict the final grain size of a material as a function of the initial microstructure. A drawback is that these techniques require extensive computer resources, especially for 3D simulations.

Acknowledgement

This research was funded by the Institute for the Promotion of Innovation through Science and Technology in Flanders (IWT-Vlaanderen).

References

- [1] Senuma T. *ISIJ Int* 2002;42:1.
- [2] Guo M, Suito H. *ISIJ Int* 1999;39:1289.
- [3] Knowlton BD, Clement JJ, Thompson CV. *J Appl Phys* 1997;81:6073.
- [4] Longworth HP, Thompson CV. *J Appl Phys* 1991;69:3929.
- [5] Smith CS. *Trans Metall Soc AIME* 1948;175:15.
- [6] Nes E, Ryum N, Hunderi O. *Acta Metall* 1985;33:11.
- [7] Hellman P, Hillert M. *Scand J Metals* 1975;4:211.
- [8] Hillert M. *Acta Metall* 1988;36:3177.
- [9] Srolovitz DJ, Anderson MP, Grest GS, Sahni PS. *Acta Metall* 1984;32:1429.
- [10] Humphreys FJ, Hatherly M. *Recrystallization and related annealing phenomena*. Oxford: Pergamon; 1996.
- [11] Manohar PA, Ferry M, Chandra T. *ISIJ Int* 1998;38:913–24.
- [12] Hillert M. *Acta Metall* 1965;13:227.
- [13] Hunderi O, Ryum N. *Acta Metall* 1982;30:739.
- [14] Abbruzzese G. *Acta Metall* 1985;33:1329.
- [15] Anderson MP, Grest GS, Doherty RD, Li K, Srolovitz DJ. *Scripta Metall* 1989;23:753.
- [16] Hassold GN, Holm EA, Srolovitz DJ. *Scripta Metall Mater* 1990;24:101.
- [17] Kad BK, Hazzledine PM. *Mater Sci Eng A* 1997;238:70.
- [18] Gao J, Thompson RG, Patterson BR. *Acta Mater* 1997;45:3653.
- [19] Soucail M, Messina R, Cosnuau A, Kubin LP. *Mater Sci Eng A* 1999;271:1.
- [20] Miodownik M, Holm EA, Hassold GN. *Scripta Mater* 2000;42:1173.
- [21] Weygand D, Bréchet Y, Lépinoux J. *Acta Mater* 1999;47:961.
- [22] Riege SP, Thompson CV, Frost HJ. *Acta Mater* 1999;47:1879.
- [23] Frost HJ, Thompson CV. *Curr Opin Solid State Mater Sci* 1996;1:361.
- [24] Miodownik M, Martin JW, Cerezo A. *Philos Mag A* 1999;79:203.
- [25] Wörner CH, Hazzledine PM. *Scripta Metall Mater* 1993;28:337.
- [26] Chen L-Q, Yang W. *Phys Rev B* 1994;50:15752.
- [27] Warren JA, Kobayashi R, Lobkovsky E, Carter WC. *Acta Mater* 2003;51:6035.
- [28] Fan D, Chen L-Q. *Acta Mater* 1997;45:611.
- [29] Fan D, Geng C, Chen L-Q. *Acta Mater* 1997;45:1115.
- [30] Chen L-Q, Fan D. *J Am Ceram Soc* 1996;79:1163.
- [31] Fan D, Chen L-Q. *Acta Mater* 1997;45:3297.
- [32] Fan D, Chen L-Q, Chen S-PP. *J Am Ceram Soc* 1998;81:526.
- [33] Moelans N, Blanpain B, Wollants P. *Acta Mater* 2005;53:1771.
- [34] Guo M, Suito H. *ISIJ Int* 1999;39:722.
- [35] Chen L-Q, Shen J. *Comp Phys Commun* 1998;108:147.
- [36] Trefethen LN. *Spectral methods in MATLAB*. Philadelphia, PA: SIAM, Society for Industrial and Applied Mathematics; 2000.
- [37] Tweed CJ, Hansen N, Ralph B. *Metall Trans A* 1983;14:2235–43.
- [38] Guo M, Suito H. *ISIJ Int* 1999;39:1297.
- [39] Ohnuma I, Ohtani H, Ishida K, Nishizawa T. *Mater Sci Forum* 1996;204:313.
- [40] Liu Y, Patterson BR. *Acta Mater* 1996;44:4327.
- [41] Palmer JE, Thompson CV, Smith HI. *J Appl Phys* 1987;62:2492.
- [42] Ringer SP, Li WB, Easterlin KE. *Acta Metall* 1989;37:831.